Geomorphology 462 (2024) 109327

Contents lists available at ScienceDirect

Geomorphology

journal homepage: www.journals.elsevier.com/geomorphology

# River linear inversion to assess drainage base-level fall history in North-western Apennines and implications on the Alessandria Basin tectonic activity

Victor Buleo Tebar [a], Mauro Bonasera [b], Simone Racano [c,*], Giandomenico Fubelli [a]

[a] Department of Earth Sciences, University of Turin, Italy
[b] Geological Survey of Italy, Italian Institute for Environmental Protection and Research (ISPRA), Italy
[c] Institute of Geosciences, University of Potsdam, Germany

ARTICLE INFO

*Keywords:*
Drainage network systems
Active tectonics
Linear inversion
Base-level fall history
Alessandria Basin
Quaternary activity

ABSTRACT

Drainage network systems are responsive elements to recent active tectonics from among all the topographic features. In geodynamically active areas, fluvial landscapes can record different processes through the formation and current presence of features related to spatial-temporal variation in base-level fall and vertical incision of stream channels. This study focuses on the tectonic evolution of the Alessandria Basin, a synorogenic tectonic basin located at the junction between the Alps and the Apennines, that experienced progressive subsidence during the overthrusting of the Monferrato Thrust Front (the westernmost outer arc of the Apennine belt) onto the Po Foreland Basin. Even though several studies have assessed the Neogene tectonic evolution at a regional scale, rates and timing of the Quaternary activity are still poorly understood in terms of both Alps/Apennines uplift and activity of the compressive front of the Monferrato Arc. In this paper, we applied the method of the river profile linear inversions to reconstruct the base-level fall history of 6 catchments that drain into the Alessandria Basin. We used nine $^{10}$Be-derived basin-average denudation rates to constrain the erodibility parameter needed to infer base-level fall rates from $\chi$-transformed river profiles. The results describe the tectonic history of the area in the last ~5 Ma, documenting increases in base-level fall rate with an initial peak between 3 and 2.5 Ma, and a second between 2 and 1.5 Ma. While the first peak is coeval with the uplift phase that involved most of the northern-central Apennine, the second one suggests an acceleration in subsidence of the Alessandria Basin concurrently with the uplift of the Monferrato Thrust Front.

## 1. Introduction

Quantitative geomorphology, studying Earth's surface landforms and processes, has evolved significantly in the modern era due to advances in techniques that enable us to decipher the complex interactions between endogenous and exogenous forces driving the landscape evolution (Burbank and Anderson, 2001; Keller and Pinter, 2002). Erosion and deposition processes are strictly linked to tectonics, climate dynamics, and the lithological characteristics of exposed landscapes (Whipple, 2004). Within this framework, the study of drainage systems assumes a primary role in investigating the evolution of the Earth's surface, identifying the dominant forces triggering these transformations, and assessing whether and how these processes have evolved over time (Burbank and Pinter, 1999; Kirby and Whipple, 2012).

In regions characterized by active or recent tectonics, drainage systems offer significant insights in characterizing the tectonic regimes and quantifying the rates of geological processes. Detachment-limited rivers, primarily bedrock drainage systems, exhibit strong sensitivity to fluctuations in base-level fall, shifts in drainage divides, and drainage captures, which may be driven by tectonic activity (García-Delgado and Velandia, 2020; Pavano and Gallen, 2021; Racano et al., 2023), climatic forcing (Whipple et al., 2017; Sharma et al., 2021; Schildgen et al., 2022; Marder and Gallen, 2023), and differential erosion (Gallen, 2018). In the case of base-level fall events, these effects can propagate upstream, manifesting as transient knickpoints that delimit the boundary between ongoing incision waves and the portion of the drainage system still in equilibrium with past configurations. The analysis of these incision waves can furnish valuable insights into the timing and the rates of events that triggered them (Bowman, 2023, and references therein).

* Corresponding author.
*E-mail address:* racano@uni-potsdam.de (S. Racano).

https://doi.org/10.1016/j.geomorph.2024.109327
Received 30 November 2023; Received in revised form 27 May 2024; Accepted 28 June 2024
Available online 30 June 2024




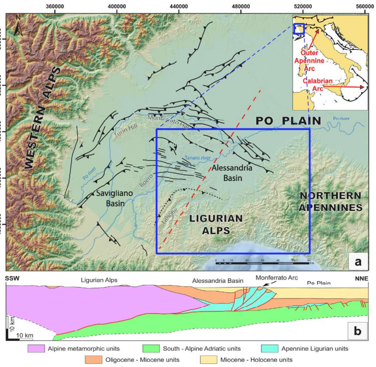


**Fig. 1.** Location of the study area and simplified tectonic framework (from Arpa Piemonte website - https://geoportale.arpa.piemonte.it/app/public/) (a). Geological cross-section along the trace of the red dashed line, modified from Irace et al., 2010 (b). (For interpretation of the references to colour in this figure legend, the reader is referred to the web version of this article.)

In tectonically active areas, and negligible eustatic fluctuations, changes in base-level fall rates can result from both uplift of catchment areas or subsidence at the catchment outlet (Racano et al., 2021; Fisher et al., 2022). The historical record of base-level fall in drainage systems can be deduced through the inversion of river profiles (Roberts and White, 2010; Goren et al., 2014). These methods enable the quantification of temporal (Goren et al., 2014; Gallen, 2018) or spatio-temporal (Fox et al., 2014; Rudge et al., 2015; Racano et al., 2023) variations in base-level fall rates, thereby providing quantitative estimations of the rates and timing of processes imprinted within drainage systems.

The northern Apennines represent an active mountain belt still undergoing compression in the outer front. This compression is driven by the shallow subduction of the Adria plate and is associated with buried active thrust in the Po Plain associated with the outermost Apennine front (Boncio and Bracone, 2009; Boccaletti et al., 2010; Faccenna et al., 2014; Livani et al., 2018; Fig. 1). This contractional tectonics has led to the formation of several foreland and thrust-top basins during the northeastward propagation of the front (Ghielmi et al., 2013, 2019).

Like most of the Apennine belt, the northern Apennines have experienced two significant phases of topographic growth. The first occurred from the late Oligocene to the late Miocene and resulted from compression following the retreat of the Adria slab subduction (Faccenna et al., 1997, 2007; Patacca et al., 1993; Royden, 1993; Wortel and Spakman, 2001). The second phase occurred during the late Pliocene – Lower Pleistocene (Galadini et al., 2003; Cosentino et al., 2017; San Jose et al., 2020; Fellin et al., 2022; Pazzaglia and Fisher, 2022) and is likely linked to mantle dynamics producing uplift, normal faulting, and opening of intermontane basins (Faccenna et al., 2014; Lanari et al., 2023). However, while the relationship between tectonics and topography evolution, as well as the timing of these processes, are well-studied and established for the eastern part of the northern Apennines (Fisher et al., 2022; Lanari et al., 2023), little is known about the rates of the tectonic episodes in the westernmost part of the region, where the Apennines connects to the Alpine belt.

Our research focuses on the Plio-Quaternary morphotectonic evolution of the westernmost part of the Po Plain, specifically in the area of the Alessandria Basin and Turin Hill, in the Piedmont Region of NW Italy (Fig. 1). This region is unique because, unlike other close areas where present geomorphological settings can be attributed to a single tectonic dynamic, the landscape results from the combined effects of uplift along the outermost Apennine belt front (Monferrato Thrust Front and Turin Hill, Pieri and Groppi, 1981; Bertotti and Mosca, 2009), and subsidence





in the Alessandria Basin, a thrust-top basin of the Monferrato Thrust Front (Irace et al., 2015; Forno et al., 2018).

Our research aims to explore how tectonic processes have contributed to shaping the drainage landscape in the western part of the northern Apennine and the timing at which these processes were most active. We applied the river inversion technique developed by Goren et al. (2014) to analyze the χ-transformed profiles of six catchments draining into the Alessandria Basin. Then, by estimating erodibility parameter using a set of published denudation rates from catchments in the central-western sector of the northern Apennines (Erlanger, 2020; Codilean et al., 2022, and references therein), we calculated base-level fall rate variations over time. Through this approach, we seek to establish connections between temporal variations in base-level fall rates and the key tectonic events that shaped the landscape of the study area during the Plio-Quaternary. Our goal is to identify possible differences in the timing and rates of the base-level fall history of the drainage system linked to the uplift and subsidence processes that shaped the westernmost sector of the northern Apennines over the Quaternary.

## 2. Geological settings

The Western Po Plain (WPP) in central-south Piedmont Region may be roughly defined as the region drained by the Po River from the base of the Southwestern Alps to the Turin Hill in the North, and by the Tanaro River and its tributaries, flowing through the Langhe, Roero, and Monferrato hills to reach the Alessandria Basin, to the south (Fig. 1). The WPP shows very changing geomorphology: the hilly systems of Turin Hill-Monferrato to the north and of the Langhe to the south, where Upper Eocene-Oligocene to Miocene rocks are exposed, and their interposed plains of Savigliano and Alessandria (Fig. 1). The landscape features are strictly connected with tectonic interactions and geomorphological processes including the Quaternary fluvio-glacial dynamics (Bonasera et al., 2019).

The WPP is characterized by a complex tectonic framework revealing the juxtaposition at a crustal-scale between the Alpine metamorphic Units and the Apennine Ligurian Units (Laubscher et al., 1992). In this region, late Eocene-Holocene predominantly siliciclastic sedimentary deposits overlay earlier deformed Alpine and Apennine formations (Mutti et al., 1995). Distinct late Eocene to late Miocene marine successions outcrop (i.e. the Tertiary Piedmont Basin (TPB) to the south and Turin Hill-Monferrato to the north). Their uppermost sequences consist of sporadic layers of evaporites and lagoon clays dating back to the Messinian (Dela Pierre et al., 2011; Irace et al., 2005; Rossi et al., 2015). The tectono-sedimentary evolution was dominated by the propagation of north-verging structures over-thrusting the Padane foreland units since Middle/Upper Miocene (Falletti et al., 1995; Piana and Polino, 1995; Bertotti and Mosca, 2009; Mosca et al., 2009). Within this context, the Savigliano Basin and Alessandria Basin depocenters evolved as subsiding basins hosting Pliocene-to-Holocene deposits with a maximum thickness of about 2000 m and 2500 m respectively. These basins are divided by the Langhe-Roero hilly region, where these successions are less than 500 m thick (Mosca, 2006; Molli et al., 2010). The Pliocene-to-Holocene deposits mask the connection between the TPB to the south and Turin Hill-Monferrato to the north. In particular, the Early Pliocene corresponds to a large-scale transgressive event recorded with upward sand-rich marginal marine deposits, onlap onto the tilted pre-Pliocene successions, indicating a return to normal marine conditions following the Messinian Salinity Crisis. After the Pliocene transgression, a regression led to the present setting of the WPP. A progressive uplift tilted the Turin Hill and Monferrato successions and deltaic to tidal plain deposits developed along the southern margins of the two basins (Boni, 1984; Carraro, 1996 and references therein). The absence of Early Pliocene layers on the foothills of Ligurian Alps led to assume that the boundary between TPB and Ligurian Alps was also morphological, already emerged from the sea since the Messinian, separating WPP from Ligurian Sea basin. The low-angle pediment, which connects Ligurian Alps with the two basins, hosted deltaic-continental deposits since Late Pliocene (Biancotti, 1979). Then, Pleistocene climate variations enhanced the development of the river networks with terrigenous sedimentation of fluvial-glacial and purely fluvial deposits received by Savigliano and Alessandria Basin (Gabert, 1960). However, although some studies have claimed the relationship between neotectonics and Quaternary variations of drainage systems (Biancotti, 1979), Quaternary fault activity is still poorly understood in this area.

The WPP is commonly recognized as a region characterized by low seismic hazard due to the absence of historical and instrumental records of significant earthquakes. This conclusion results from the combination of two factors: firstly, the historical earthquake record, which displays a relatively limited number of moderate-to-high magnitude events, with the most recent occurring during the Middle Ages (Bonasera et al., 2021); secondly, the scarcity of dedicated research on earthquake geology in this area. While numerous studies have highlighted local Quaternary tectonics, very few have interpreted the observed evidence in terms of seismic hazard. Nonetheless, recent research provides indications of active faulting and potential paleo-seismic activity during the Middle Pleistocene to Holocene epochs (Frigerio et al., 2017; Bonasera et al., 2022).

## 3. Methods

### 3.1. Stream power model framework

The model that describes the evolution of river profiles is based on the relation between erosion ($E$) and rock uplift ($U$) that defines the change in elevation of a point along the channel through time:

$$\frac{dz(t,x)}{dt} = U(t,x) - E(t,x) \quad (1)$$

The erosion rate of a bedrock channel can be defined by the stream power equation:

$$E = KA(x)^m S(t,x)^n \quad (2)$$

where $A$ is the upstream drainage area, $S$ is the channel slope, and $K$ is the erodibility coefficient that depends on different parameters such as lithology, rock deformation, and climate, $m$ and $n$ are both positive coefficients for parameters related to basin hydrology and erosion processes in the channel (Howard, 1994; Whipple and Tucker, 1999). For those rivers with longitudinal profiles that describe a relatively steady-state equilibrium between rock uplift and erosion processes ($U = E$), the following empirical power-law represents the relationship between channel slope ($S$) and upstream drainage area ($A$):

$$S = \left(\frac{E(orU)}{K}\right)^{\frac{1}{n}} A^{\frac{m}{n}} \quad (3)$$

where $m/n$ corresponds to the concavity index, an empirical exponent whose values are commonly between 0.3 and 0.6 in steady-states profiles conditions (Tucker and Whipple, 2002; Kirby and Whipple, 2012). Eq. (3) can be used to derive the channel steepness index ($k_s$):

$$k_s = SA^{\frac{m}{m}} = \left(\frac{E(or\ U)}{K}\right)^{\frac{1}{n}} \quad (4)$$

By applying a uniform $m/n$ to a regional drainage system, we obtain the normalized steepness index ($k_{sn}$), which is a robust measure of relative channel steepness throughout a region (Wobus et al., 2006).

For $n$ equal to 1 (linearity between channel slope and erosion processes), steady-state conditions ($U = E$), no substantial changes in the drainage basin area through time (e.g., via drainage capture), and a spatially and temporally uniform $K$, Eq. (3) can be integrated for the upstream drainage area to predict the elevation of the river profile





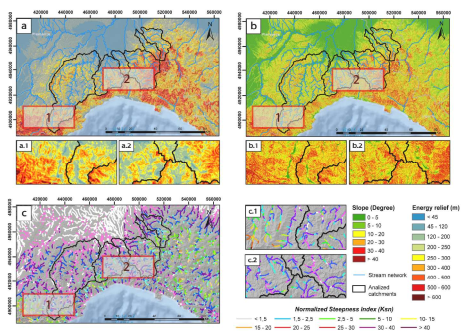


**Fig. 2.** Multi-criteria analysis (Energy relief (a), Slope (b), and Normalized Steepness Index to a reference concavity of 0.36 (c)) of the stability conditions of the analyzed catchments with a particular focus on their boundaries and their divides (0.1 and 0.2).

$$z(x) = \int_{-\tau(x)}^{0} U(t')dt' \quad (5)$$

where $\tau$ is the integrand quantity defining the travel-time of a perturbation along a river profile (Whipple and Tucker, 1999):

$$\tau = \int_0^x \frac{dx'}{K(x')A(x')^m} \quad (6)$$

### 3.2. Base-level fall histories from river profile linear inversion

Eq. (5) can be simplified to define the equation of the $\tau$-plot:

$$z(x) = z(x_b) + U\tau \quad (7)$$

where $z(x_b)$ is the elevation of the catchment outlet, and the slope of the equation is the base-level fall rate, represented by $U$ (Gallen, 2018; Racano et al., 2021).

This equation can be inverted to extract temporal (Pritchard et al., 2009; Goren et al., 2014; Gallen, 2018) or spatiotemporal (Fox et al., 2014; McNab et al., 2018; Quye-Sawyer et al., 2020) variations in base-level fall histories (equivalent to catchment rock-uplift relative to the outlet). However, this approach requires knowing the erosion coefficient $K$ to estimate $\tau$.

Eq. (5) can be simplified in a $K$-independent form of $\tau$ called $\chi$, obtained by removing $K$ from Eq. (6) (Perron and Royden, 2013, Royden and Perron, 2013):

$$\chi = \int_{x_b}^{x} \left(\frac{A_0}{A(x')}\right)^{\frac{m}{n}} dx' \quad (8)$$

$\chi$ has units of length, and $A_0$ is a reference drainage area. This integral is used to define the $\chi$-plot:

$$z(x) = z(x_b) + \left(\frac{E(orU)}{KA_0^m}\right)^{\frac{1}{n}} \chi \quad (9)$$

By taking $A_0 = 1$, the slope of Eq. (8) is represented by the river steepness index (Smith et al., 2022), and can be simplified as:

$$z(x) = z(x_b) + k_{s(n)}\chi \quad (10)$$

where $k_{s(n)}$ is a non-dimensional estimate of $U$.

Following Goren et al. (2014), we can estimate the non-dimension base-level fall history of river networks for discrete $\chi$-intervals using Eq. (10) and assuming block-uplift conditions. The data organization assumes that $N$ data points of $z$ and $\chi$ along the fluvial network are ordered according to elevation assuming that every stream channel shares a common rock-uplift history at the same $\chi$ value (Goren et al., 2014; Gallen, 2018). By this discretization, Eq. (10) can be organized in matrix form:

$$A^* U^* = z \quad (11)$$

where $\mathbf{A}^*$ is an $N\ x\ q$ matrix, $q$ is the number of $\chi$ intervals, $\mathbf{U}^*$ is the non-dimensional uplift (equivalent to $k_{sn}$ if $A_0 = 1$), and $\mathbf{z}$ is the elevation. This is an overdetermined inverse problem, as there are more known

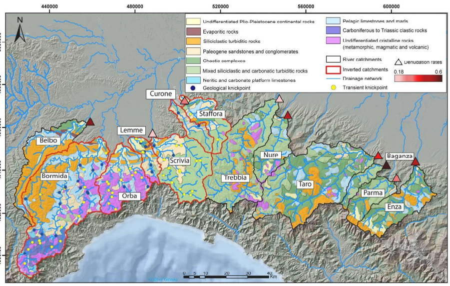


**Fig. 3.** Lithological map of the catchments selected for river linear inversion and of the catchments with $^{10}$Be average denudation rates, provided by the OCTOPUS V2 database (Codilean et al., 2022) and from Erlanger (2020), used for the calculation of the erodibility parameter (*K*). Triangles indicate the location of TCN samples, and their colour gradient is proportional to the estimated denudation rate. Knickpoints are represented by circles within the analyzed catchments and colored by their classification.

data points than unknown parameters. As such, a least-squares estimate for **U*** is used:

$$\mathbf{U}^* = \mathbf{U}^*_{pri} + \left(\mathbf{A}^{*T}\mathbf{A}^* + \Gamma^2\mathbf{I}\right)^{-1}\mathbf{A}^{*T}\left(\mathbf{z} - \mathbf{A}^*\mathbf{U}^*_{pri}\right) \quad (12)$$

where $\Gamma$ is a dampening coefficient that determines the smoothness imposed on the solution, **I** is the $q \times q$ identity matrix and $\mathbf{U}^*_{pri}$ represents the prior guess for **U*** estimated from the average slope of the $\chi$-plot.

Eq. (12) can also be applied to Eq. (7) to directly derive the base-level fall rate (Gallen, 2018; Racano et al., 2021). The use of $\tau$ instead of $\chi$ allows not only the direct estimation of the rock uplift from linear inversion, but also the use of rock-variable *K* to convert $\chi$ coordinates in relation to the rocks that channels cut (Gallen, 2018; Pazzaglia and Fisher, 2022; Fisher et al., 2022).

Once estimated *K*, $\chi$ and $U^*$ can be converted in $\tau$ and base-level fall rate by the equations:

$$E(U) = U^* K A_0^m \quad (13)$$

$$\tau = \frac{\chi}{K A_0^m} \quad (14)$$

where *K* can be derived from Eq. (4):

$$K = \frac{E(U)}{k_{s(n)}} \quad (15)$$

### 3.3. River inversion setup and estimation of K

We applied linear inversions in six catchments that drain into the Alessandria Basin from the Alps-Apennine junction, aiming to reconstruct base-level fall events triggered by the subsidence at the catchment outlets and/or the uplift of the mountain belt. Selected catchments drain the Ligurian Alps and the westernmost tip of the northern Apennine belt to the Alessandria Basin – Po Plain. Catchments show evidence of general present (Fig. 2) and past (over the last 3 Myr, Lanari et al., 2023) divide stability, a condition needed to apply river inversion (Racano et al., 2021, 2023). We extracted stream channels by using the MATLAB® toolbox TopoToolbox (Schwanghart and Scherler, 2014) as well as for the calculation of the erodibility coefficient, knickpoint extraction, and river profile inversions. The distinction between geological and transient knickpoints was made based on the proximity of each knickpoint to every lithological contact (Fig. 3). The concavity index used to estimate $\chi$ has been calculated by finding the best value among 0 and 1 that minimize the scatter in the $\chi$-plots of the inverted catchments (Goren et al., 2014), and computing the catchments average, obtaining the value of 0.36 (Table 1, Fig. S5). The digital elevation model used for this study was the open-source Copernicus Global Digital Surface Model with a spatial resolution of 30 m/px. In order to prevent and reduce the noise of the results from the inversions, we imposed a minimum drainage area of 1 km$^2$ and removed streams shorter than 5 km. In addition, we smoothed the elevations of the longitudinal river profiles by applying the Constrained Regularized Smoothing (CRS) method (Schwanghart and Scherler, 2014). The $\chi$-increments to apply the liner inversion ($\chi$-steps = 11) has been estimated by finding the number of $\chi$-steps that minimize the misfit between real and modeled river elevations (Fig. S6, Fig. S7) (Racano et al., 2023; Clementucci et al., 2023).

We estimated the erodibility parameter (*K*) by a set of $^{10}$Be- derived denudation rates available from Erlanger (2020) and from the OCTOPUS





**Table 1**
concavity and average $k_{sn}$ of the catchment used to estimate *K* (a) and to apply the river linear inversion (b). Catchments (a) are those where $^{10}$Be derived denudation rates have been estimated ((c) OCTOPUS V2 database – Codilean et al., 2022, (d) Erlanger, 2020) and used in this paper to estimate *K*. Concavity index has been estimated by finding the best value that reduces the scatter of $\chi$ - z data (Goren et al., 2014).

| Catchment | Concavity ($m/n$) | Mean $k_{sn}$ ($m^{0.72}$) | Denudation (mm/yr) | $K$ ($m^{0.28}$ $yr^{-1}$) | $K_{error}$ ($m^{0.28}$ $yr^{-1}$) |
|---|---|---|---|---|---|
| Belbo *a* | 0.41 | 17.8 ± 6.7 | 0.500 ± 0.153 *c* | 2.82 × $10^{-5}$ | 1.38 × $10^{-8}$ |
| Bormida *b* | 0.47 | 9,1 ± 2,00 | N/D | N/D | N/D |
| Orba *b* | 0.4 | 11,3 ± 3,2 | N/D | N/D | N/D |
| Lemme *b* | 0.37 | 7,65 ± 3,3 | N/D | N/D | N/D |
| Scrivia *a b* | 0.35 | 5.7 ± 3.6 | 0.185 ± 0.042 *c* | 3.25 × $10^{-5}$ | 2.21 × $10^{-8}$ |
| Curone *b* | 0.34 | 15,6 ± 5,7 | N/D | N/D | N/D |
| Staffora *a b* | 0.48 | 13.8 ± 5.1 | 0.234 ± 0.041 *d* | 1.69 × $10^{-5}$ | 6.97 × $10^{-9}$ |
| Trebbia *a* | 0.38 | 12.8 ± 6.3 | 0.184 ± 0.042 *c* | 1.44 × $10^{-5}$ | 7.85 × $10^{-9}$ |
| Nure *a* | 0.24 | 20.9 ± 6.1 | 0.443 ± 0.245 *c* | 2.11 × $10^{-5}$ | 1.32 × $10^{-8}$ |
| Taro *a* | 0.38 | 22.2 ± 6.1 | 0.382 ± 0.072 *d* | 1.72 × $10^{-5}$ | 5.75 × $10^{-9}$ |
| Baganza *a* | 0.27 | 17.4 ± 5.4 | 0.608 ± 0.164 *c* | 3.50 × $10^{-5}$ | 1.45 × $10^{-8}$ |
| Parma *a* | 0.2 | 18.9 ± 4.4 | 0.277 ± 0.109 *d* | 1.47 × $10^{-5}$ | 6.70 × $10^{-9}$ |
| Enza *a* | 0.31 | 21.6 ± 5.3 | 0.435 ± 0.076 *d* | 2.02 × $10^{-5}$ | 6.11 × $10^{-9}$ |

database (Codilean et al., 2022, and references therein) spanning all the length of the northern flank of the Northern Apennine draining in the Po Plain (Fig. 3, Table 1). We applied Eq. (15) (assuming *n* equal to 1) to derive *K* (1) for each catchment by dividing denudation rates for the average $k_{sn}$ upstream the sampling locations, and (2) from the linear fit of the $k_{sn}$ vs *E* (Fig. 4c). The linear fit has been made by weighting the errors both on *x* and *y* (York et al., 2004). Plots of $k_{sn}$ and *K* have been made by using RStudio. Finally, we converted $\chi$ in $\tau$ and $U^*$ in base-level fall rate by applying the estimated *K* values to Eqs. (13) and (14).

Unlike Fisher et al. (2022), who employ a lithology-based binning of the catchments to estimate *K* along the external margin of the northern Apennines, we opted for the method of averaging *K* values across the investigated catchments. This choice was guided by two primary considerations. Firstly, $^{10}$Be denudation rates are tied to lithologies contributing to the quartz content in sediments, making it unsuitable for estimating *K* for rocks without quartz (such as limestones) (Fig. S1). Secondly, the lithological *K*-dependent approach assumes that the boundaries between lithologies remain stable over time. However, this condition is easily violated as the positions of rock boundaries depend on their geometry, and lithological knickpoints can even migrate over time or be generated by progressively eroding new lithologies (Fig. S2).

## 4. Results

### 4.1. Rock average normalized steepness index ($k_{sn}$) and erodibility coefficient (K) estimation

The average denudation rates (Erlanger, 2020; Codilean et al., 2022) across the nine catchments considered for estimating the *K* value range from 0.185 to 0.608 mm/yr (Table 1, Fig. 3). This trend generally exhibits an eastward increase in rates, mirroring the pattern also observed in the catchment average $k_{sn}$ values (Fig. 4c). In general, catchments characterized by higher $k_{sn}$ predominantly feature Chaotic complex and Clastic turbiditic rocks compared to other catchments (Figs. 3, 4a). However, even though clastic turbidite rocks exhibit a slightly higher average value for channel normalized steepness index, they also display higher variability in $k_{sn}$ values, with the range encompassing the average $k_{sn}$ of all other lithologies (Fig. a).

The erodibility parameter *K*, estimated for each catchment with denudation rate data (Table 1, Fig. 4 b), generally shows low variability over the average. Only Belbo, Scrivia, and Baganza catchments show average values higher than those of the other catchments, but their error ranges fall within the $K_{mean}$ of the plot ($2.034 \times 10^{-5} \pm 9.341 \times 10^{-6}$).

The average *K* estimated from the individual catchment aligns closely with the slope of the linear fit derived from plotting the catchment average $k_{sn}$ against the corresponding denudation rates ($2.117 \times 10^{-5} \pm 2.25 \times 10^{-6}$) (Fig. 4c). The data indicates a good linear fit passing from the origin of the axis (R2 of 0.91), with only the values for Scrivia and Baganza catchments deviating outside the linear fit.

### 4.2. Fluvial inversion

River linear inversion results reveal comparable estimates of $\tau$ and temporal variations in base-level fall (Fig. 5). The oldest $\tau$ values average between 2.5 and 3.5 Myr, except for the Bormida catchment, the largest one located on the western margin of the Alessandria Basin, which exhibits the oldest base-level fall history, reaching back to 5.65 Ma.

All base-level fall rates range from a minimum of 0.1 to a maximum of 0.9 mm/yr, displaying two peaks between 3 and 2.5 Myr, and between 2 and 1.5 Myr. These base-level fall peaks are less prominent for the Bormida catchment, where the older peak predates those in other catchments by 4 Myr. In contrast, the easternmost catchments (Curone and Staffora) show more pronounced peaks, reaching the highest base-level fall rates.

Most of the catchments (Orba, Lemme, Scrivia, and Staffora) also show a slight increase in base-level fall rates around or shortly after 1 Ma. However, the overall trend for all the analyzed catchments indicates a decrease in rates after 2 Ma, with average values for the younger ages never exceeding 0.2 mm/yr. Transient knickpoints along river profiles display a moderate correlation with variations in base-level fall rates in most of the analyzed catchments, tending to cluster in correspondence with the peaks of the base-level curves (Fig. 5).

## 5. Discussion

### 5.1. Reliability of the river profile linear inversion

The linear fit of the $k_{sn}$ vs. denudation rates (Fig. 4c) passes through the axis origin without forcing. This is concordant with a linear correlation between erosional processes and channel gradient, and supports the assumption of *n* equal to 1 (Racano et al., 2021, 2023).

The use of a catchment average *K*, and not linked to the eroded lithologies, stands as a reasonable approximation. The representative average $k_{sn}$ values for the main outcropping lithologies (Fig. 4a) show low variability, even when comparing crystalline rocks with sedimentary ones. Only siliciclastic turbidites show a significantly higher average $k_{sn}$ value. However, this seems to exert a negligible impact on *K* and on the shapes of river profiles.

Among the three catchments with relatively higher *K* values (Belbo, Scrivia, and Baganza, Fig. 4b), only the Belbo catchment is predominantly composed of siliciclastic turbidites (Fig. 3), while the other two are dominated by mixed siliciclastic and carbonatic turbidites. Belbo and Baganza catchments share a narrow shape and the highest denudation rates (Fig. 3), despite the other catchments that have wider catchment areas. This feature could link their different *K* values to the different geometric characteristics they have. However, this argument does not hold for the Scrivia catchment, which shows a catchment shape not significantly different from the others.

The minimal impact of lithological variations on river profile shapes





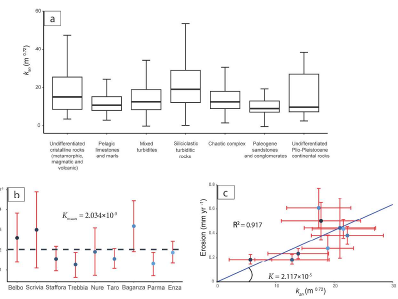


**Fig. 4.** (a) Boxplots of the catchment's average $k_{sn}$ metrics for the lithological units classified in the analyzed catchments. (b) *K* values calculated for each catchment where 10Be denudation rates are provided, by following Eq. (15), and dashed line representing the $K_{mean}$ value of the plot. (c) Linear York fit of the $k_{sn}$ vs denudation rate plot. The colour of the circles follows the west-to-east longitude gradient.

is further evident in Fig. 5. Lithological knickpoints do not appear to exert a strong influence on base-level fall trends, and the shape of river profiles lacks evident slope breaks where lithological knickpoints are mapped. Conversely, transient knickpoints, particularly in Bormida, Orba, Lemme, and Staffora catchments tend to cluster in correspondence to main base-level fall variations. All these features support, in the case of catchments draining into the Alessandria Basin, the suitability of using a catchment average *K* for calibrating river inversions.

### 5.2. Subsidence history of the Alessandria Basin and implication for the Monferrato Thrust Front evolution

While a significant uplift phase has been documented in the northern-central Apennine belt between 3 and 2.5 Ma (Galadini et al., 2003; Cosentino et al., 2017; San Jose et al., 2020; Fellin et al., 2022; Pazzaglia and Fisher, 2022), there is a lack of data regarding the potential influence of this uplift pulse in the region connecting the Alps and the Apennines, at least in terms of magnitude and timing of the events. Most of the investigated catchments reveal an acceleration in base-level fall rates from or soon after 3 Ma, aligning with the onset of the last uplift phase of the Apennine belt. Notably, the rates of base-level fall follow a westward decreasing trend, suggesting a potential decrease in the influence of this uplift pulse moving from the Apennine to the Alps. Like in other areas of the Apennine belt where both stratigraphic (Cosentino et al., 2017, and references therein) and geochemical data (e.g., San Jose et al., 2020; Fellin et al., 2022) support the onset of accelerated uplift after 3 Ma, the combined base-level fall history from all the analyzed catchments (Fig. 6) suggest that this accelerated uplift event also involved the westernmost part of the northern Apennine belt and the junction with the Alps.

Our results are also supported by local tectonic and stratigraphic interpretations from published scientific literature. The area already relied on emerged reliefs (Torino and Monferrato Hills) during the Early Pliocene, while the current alluvial plains, Savigliano and Alessandria Basins, were occupied by the remains of the ancient Ligurian Sea (Carraro, 1996). A Zanclean shoreline (5.3–3.6 Ma) was located along the current Torino and Monferrato reliefs (Bonasera et al., 2019), intersecting the terminal parts of some of the analyzed catchments in this study (Fig. 7a), at a current average altitude of 240 ± 80 m.a.s.l. During the upper Pliocene (3.6–2.5), the shoreline experienced a regression due to a combination of climatic transition and a tectonic event affecting the western sector of TPB and the compressive NW-verging Torino and Monferrato Hills fronts, located at a current average altitude of 219 ± 70 m.a.s.l (Vigna et al., 2010). The Alessandria Basin in this period was characterized by the widespread deposition of materials derived from the erosion of the uplifted reliefs in the southern part of the basin margin (Irace et al., 2015). As a result of this tectonic framework, the Pliocene-Pleistocene succession is characterized by a sequence of transgressive-regressive fluctuations with the presence of deep marine clays, shallow-marine systems, sands from deltaic environment and continental gravels, sands and clays (Carraro, 1996; Vigna et al., 2010; Irace et al., 2010; Irace et al., 2015). In addition, studied fluvial successions show erosional unconformities of fluvial units along the southern margin of the basin during the Plio-Pleistocene transition between 2.8 and 2.58 Ma (Irace et al., 2015).

Fluvial profile inversions reveal an initial peak in base-level fall after 3 Ma in every catchment, except for Bormida catchment, where the older base-level fall peak predates 3.5 Ma, and Lemme catchment, where





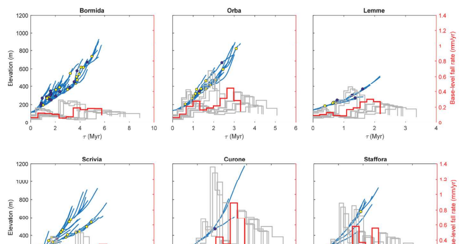


**Fig. 5.** τ-plots, knickpoints, and base-level fall history of the six selected catchments selected to apply the river linear inversion. Red stairs correspond to the average of the nine different *K* values calculated for each denudation rate (grey stairs). (For interpretation of the references to colour in this figure legend, the reader is referred to the web version of this article.)

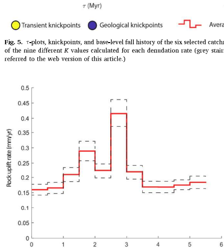


**Fig. 6.** Rock uplift rate calculated with the average of base-level fall variations among the six analyzed catchments for a 0.25 Myr time interval. Average values are represented by the red line, whereas the errors by the dashed line. (For interpretation of the references to colour in this figure legend, the reader is referred to the web version of this article.)

τ does not exceed 2.1 Myr (Fig. 5). These results align with the presence of unconformities in fluvial units along the southern margin, likely associated with the subsidence of the Alessandria Basin during this period. Given that the Alessandria Basin represents the thrust-top basin of the Monferrato Thrust Front, the uplift of the Zanclean shoreline of the Turin Hill (Fig. 7a) corresponds to the onset of the older acceleration in the base-level fall rate. This confirms a coupling between subsidence in the Alessandria Basin and the uplift of the Monferrato Thrust Front as also suggested by the modeled top – Zanclean surface (Fig. 7a, Bonasera et al., 2019). Moreover, base-level fall episodes recorded by Curone and Staffora are more prominent than in the other catchments. As the easternmost catchments in the study area drain into the foreland Po Basin and close to the thrust front (Bigi et al., 1990), rather than the Alessandria Basin, these higher base-level peaks may suggest faster subsidence in the flexure foreland compared to the thrust-top basin, or faster uplift of the drained mountain belt linked to the regional uplift involving all the chain at that time (Cosentino et al., 2017; San Jose et al., 2020; Fellin et al., 2022). In general, according to the hypothesis that the boundary between the Pliocene and Pleistocene represents the moment when uplift started accelerating in most of the northern-central Apennine (Lanari et al., 2023, and references therein), the concurrent acceleration of the base-level fall rate in the Piedmont region could potentially be influenced by this event. Notably, during the Early Pleistocene, while most of the north-central Apennines were experiencing vertical tectonics, our data also suggest a potential contractional reactivation of one of the outermost compressive fronts of the Apennine belt.

A second base-level fall peak inferred by the combined base-level fall

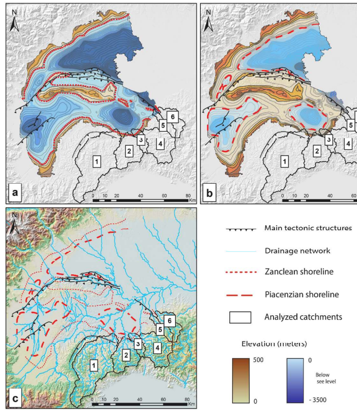


**Fig. 7.** depth of the top Zanclean (a) and top Piacenzian (b) surfaces inferred from seismic data modeling (modified from Bonasera et al., 2019), and location of the associated basin shorelines. Present settings of the study area (c), with the modern location of the uplifted shorelines. (1) Bormida; (2) Orba; (3) Lemme; (4) Scrivia; (5) Curone; (6) Staffora.

histories (Fig. 6) suggests another event of uplift acceleration between 2 and 1.5 Ma. The interpretation of this second event is more complex, as no coeval accelerated uplift phases are recorded in other areas of the Apennine belt. After 2.5 Ma, the study area experienced a second uplift pulse, as demonstrated by a second uplifted shoreline in the Alessandria and Savigliano Basins dated to the upper Pliocene (Fig. 7b, Irace et al., 2015). The two basins were disconnected by a topographic high, likely linked to the previous activation of the Monferrato Thrust Front (Fig. 7b). Since the Alessandria Basin still represents a depocenter of the investigated catchments, the younger base-level fall peak can be potentially linked to a local tectonic event triggered by the reactivation of the Alessandria Basin – Monferrato Thrust Front system, but further investigations are needed to support this hypothesis.

After the second base-level fall event, the general trend indicates a decrease in rates over time. Some catchments (Orba, Lemme, Scrivia, and Staffora) (Fig. 5) record a base-level fall peak around 1 Ma, but it does not have any clear correlation with any known tectonic event, and is not systematically recorded in all the analyzed catchments, suggesting that other potential causes (e.g. climatic variations) may have generated it. In general, the processes that produced the 3 and 2–1.5 base-level fall events have either stopped or are no longer as strong to produce significant perturbations in the drainage system.

## 6. Conclusions

The study we carried out on the catchments draining the Ligurian Alps and the westernmost tip of the Northern Apennine to the Alessandria Basin provides new significant insights into the evolution of the study area over the last 3 million years. We demonstrated how the application of linear inversion of river profiles to extract base-level fall histories can be a powerful tool not only to derive rock uplift of studied catchments, but also the history related to subsidence at catchment





outlets.

Our findings shed new light on the timing and rates of evolution in the Alessandria thrust-top basin and, consequently, on the evolution of the Monferrato Thrust Front, which represents the westernmost outer wedge of the Northern Apennine Belt. The base-level fall history of the investigated catchments reveals that this thrust-top basin/contractional arc system was active during the last strong uplift phase that involved the northern and central Apennine from the late Pliocene/early Pleistocene, indicating propagation of this uplift pulse until the junction with the Alps. A second event occurring between 2 and 1.5 Ma could potentially be interpreted as the result of local tectonics triggered by accelerated subsidence of the Alessandria Basin and uplift of the Turin Hill, likely associated with the reactivation of the Monferrato thrust.

The latest base-level fall stages suggest a decrease in the rates of these phenomena, which does not necessarily imply a halt in the tectonic processes in the area (where moderate seismic activity is still recorded). Rather, it suggests that the tectonic processes affecting the Monferrato Thrust Front system do not significantly influence recent drainage system settings.

## CRediT authorship contribution statement

**Victor Buleo Tebar:** Writing – review & editing, Writing – original draft, Software, Methodology, Investigation, Formal analysis, Data curation, Conceptualization. **Mauro Bonasera:** Writing – review & editing, Validation, Supervision, Investigation, Conceptualization. **Simone Racano:** Writing – review & editing, Validation, Supervision, Conceptualization. **Giandomenico Fubelli:** Writing – review & editing, Supervision, Conceptualization.

## Declaration of competing interest

The authors declare that they have no known competing financial interests or personal relationships that could have appeared to influence the work reported in this paper.

## Data availability

No data was used for the research described in the article.

## Acknowledgments

We thank the Executive Guest Editor Prof. Efthimios Karymbalis and the two anonymous reviewers for their constructive comments and suggestions, which improved the quality of this manuscript.

## Appendix A. Supplementary data

Supplementary data to this article can be found online at https://doi.org/10.1016/j.geomorph.2024.109327.

## References

Bertotti, G., Mosca, P., 2009. Late-orogenic vertical movements within the arc of the SW Alps and Ligurian Alps. Tectonophysics 475 (1), 117–127. https://doi.org/10.1016/j.tecto.2008.08.016.

Biancotti, A., 1979. Il quaternario dell'area compresa fra Stura di Demonte e Tanaro (Piemonte sud-occidentale). Accademia Nazionale dei Lincei Rendiconti della Classe di Scienze fisiche, matematiche e naturali 3 (66), 1–10.

Bigi, G., Cosentino, D., Parotto, M., Sartori, R., Scandone, P., 1990. Structural model of Italy. Scale 1:500.000. In: Progetto Finalizzato Geodinamica. C.N.R, Florence.

Boccaletti, M., Corti, G., Martelli, L., 2010. Recent and active tectonics of the external zone of the Northern Apennines (Italy). Int. J. Earth Sci. 100, 1331–1348. https://doi.org/10.1007/s00531-010-0545-y.

Bonasera M., Redana M., Fubelli G., Racano S., Mosca P., Fioraso G., and Cattarossi W. (2019). Quaternary morphotectonic evolution of the Western Po Plain (North-Western Italy). Regional Conference on Geomorphology, Athens (Greece), September 19–21.

Bonasera, M., Redana, M., Fubelli, G., 2021. Historical seismic catalogue updates and site effects considerations for southern Piedmont (Northwest Italy). Rend. Online Soc. Geol. Ital. 55, 2–9. https://doi.org/10.3301/ROL.2021.09.

Bonasera, M., Fubelli, G., Comina, C., Bosco, F., Umili, G., Zorloni, L., Francesco, P., 2022. A multidisciplinary approach to detect the seismogenic source of the Tortona 1828 earthquake (Piedmont, Northwest Italy). Ital. J. Geosci. 141 (1), 69–83. https://doi.org/10.3301/IJG.2022.07.

Boncio, P., Bracone, V., 2009. Active stress from earthquake focal mechanisms along the Padan-Adriatic side of the Northern Apennines (Italy), with considerations on stress magnitudes and pore fluid pressures. Tectonophysics 476, 180–194. https://doi.org/10.1016/j.tecto.2008.09.018.

Boni, A., 1984. Il Pliocene e la neotettonica nelle Alpi Liguri. Mem. Soc. Geol. Ital. 28, 229–265.

Bowman, D., 2023. Knickpoint retreat. In: Bowman, D. (Ed.), Base-level Impact: A Geomorphic Approach. Springer International Publishing, Cham, pp. 49–57. https://doi.org/10.1007/978-3-031-24994-5_7.

Burbank, D.W., Anderson, R.S., 2001. Tectonic Geomorphology. Blackwell Science, Malden, p. 273.

Burbank, D.W., Pinter, N., 1999. Landscape evolution: the interaction of tectonics and surface processes. Basin Res. 11, 1–6. https://doi.org/10.1046/j.1365-2117.1999.00089.x.

Carraro, F., 1996. Revisione del Villafranchiano nell'area tipo di Villafranca d'Asti. Il Quaternario 9 (1), 5–119.

Clementucci, R., Ballato, P., Siame, L.L., Faccenna, C., Racano, S., Torreti, G., Lanari, R., Leanni, L., Guillou, V., 2023. Transient response to changes in uplift rates in the northern Atlas-Meseta system (Morocco). Geomorphology 435. https://doi.org/10.2139/ssrn.4263924.

Codilean, A.T., Munack, H., Saktura, W.M., Cohen, T.J., Jacobs, Z., Ulm, S., Hesse, P.P., Heyman, J., Peters, K.J., Williams, A.N., Saktura, R.B.K., Rui, X., Chishiro-Dennelly, K., Panta, A., 2022. OCTOPUS database (v.2). Earth Syst. Sci. Data 14 (8), 3695–3713. https://doi.org/10.5194/essd-14-3695-2022.

Cosentino, D., Asti, R., Nocentini, M., Gliozzi, E., Kotsakis, T., Mattei, M., Esu, D., Spadi, M., Tallini, M., Cifelli, F., Pennacchioni, M., Cavuoto, G., Di Fiore, V., 2017. New insights into the onset and evolution of the central Apennine extensional intermontane basins based on the tectonically active L'Aquila Basin (Central Italy). GSA Bull. 129 (9–10), 1314–1336. https://doi.org/10.1130/B31679.1.

Dela Pierre, F., Bernardi, E., Cavagna, S., Clari, P., Gennari, R., Irace, A., Lozar, F., Lugli, S., Manzi, V., Natalicchio, M., Roveri, M., Violanti, D., 2011. The record of the Messinian salinity crisis in the Tertiary Piedmont Basin (NW Italy): the Alba section revisited. Paleogeogr. Paleoclimatol. Paleoecol. 310, 238–255. https://doi.org/10.1016/j.paleo.2011.07.017.

Erlanger, E. (2020). Erosion and weathering of the Northern Apennines with implications for the tectonics and kinematics of the orogen [PhD thesis, ETH Zurich] ETH library. doi:https://doi.org/10.3929/ethz-b-000393261.

Faccenna, C., Mattei, M., Funiciello, R., Jolivet, L., 1997. Styles of back-arc extension in the Central Mediterranean. Terra Nova 9 (3), 126–130. https://doi.org/10.1046/j.1365-3121.1997.d01-12.x.

Faccenna, C., Funiciello, F., Civetta, L., D'Antonio, M., Moroni, M., Piromallo, C., 2007. Slab disruption, mantle circulation, and the opening of the Tyrrhenian basins. Geol. Soc. Am. Spec. Pap. 418 https://doi.org/10.1130/2007.2418(08).

Faccenna, C., Becker, T.W., Auer, L., Billi, A., Boschi, L., Brun, J.P., Capitanio, F.A., Funiciello, F., Horvàth, F., Jolivet, L., Piromallo, C., Royden, L., Rossetti, F., Serpelloni, E., 2014. Mantle dynamics in the Mediterranean. Rev. Geophys. 52, 283–332. https://doi.org/10.1002/2013RG000444.

Falletti, P., Gelati, R., Rogledi, S., 1995. Oligo-Miocene evolution of Monferrato and Langhe, related to deep structures. In: Polino, R., Sacchi, R. (Eds.), Rapporti Alpi Appennino, vol. 14. Accademia Nazionale delle Scienze, Roma, pp. 1–19.

Fellin, M.G., San Jose, M., Faccenna, C., Willett, S.D., Consentino, D., Lanari, R., Gourbet, L., Maden, C., 2022. Transition from slab roll-back to slab break-off in the central Apennines, Italy: Constraints from the stratigraphic and thermochronologic record. GSA Bull. 134 (7/8), 1916–1930. https://doi.org/10.1130/B36123.1.

Fisher, J.A., Pazzaglia, F.J., Anastasio, D.J., Gallen, S.F., 2022. Linear inversion of fluvial topography in the Northern Apennines: Comparison of base-level fall to crustal shortening. Tectonics 41, e2022TC007379. https://doi.org/10.1029/2022TC007379.

Forno, M.G., De Luca, D., Bonasera, M., Bucci, A., Gianotti, F., Lasagna, M., Lucchesi, S., Pelizza, S., Piana, F., Taddia, G., 2018. Synthesis on the Turin subsoil stratigraphy and hydrogeology (NW Italy). Alp. Mediterr. Quat. 31 (2), 147–170. https://doi.org/10.26382/AMQ.2018.10.

Fox, M., Goren, L., May, D.A., and Willett, S.D. (2014). Inversion of fluvial channels for paleorock uplift rates in Taiwan. J. Geophys. Res. Earth, 119(9), 1853–1875. doi: https://doi.org/10.1002/2014JF003196.

Frigerio, C., Bonadeo, L., Zerboni, A., Livio, F., Ferrario, M.F., Fioraso, G., Irace, A., Brunamonte, F., Michetti, A.M., 2017. First evidence for late Pleistocene to Holocene earthquake surface faulting in the Eastern Monferrato Arc (Northern Italy): Geology, pedostratigraphy and structural study of the Pecetto di Valenza site. Quat. Int. 40, 1–22. https://doi.org/10.1016/j.quaint.2016.12.022.

Gabert, P., 1960. Les plaines occidentales du Pô et leurs piédmonts (Piémont, Lombardie occidentale et centrale), étude morphologique (Thèse de Doctorat d'État). Imprimerie Louis Jean, Gap, p. 531.

Galadini, F., Galli, P., Moro, M., 2003. Paleoseismology of silent faults in the Central Apennines (Italy): the Campo Imperatore Fault (Gran Sasso Range Fault System). Ann. Geophys. 46 (5) https://doi.org/10.4401/ag-3456.

Gallen, S.F., 2018. Lithologic controls on landscape dynamics and aquatic species evolution in post-orogenic mountains. Earth Planet. Sci. Lett. 493, 150–160. https://doi.org/10.1016/j.epsl.2018.04.029.





García-Delgado, H., Velandia, F., 2020. Tectonic geomorphology of the Serranía de San Lucas (Central Cordillera); Regional implications for active tectonics and drainage rearrangement in the Northern Andes. Geomorphology 349, 106914. https://doi.org/10.1016/j.geomorph.2019.106914.

Ghielmi, M., Minervini, M., Nini, C., Rogledi, S., Rossi, M., 2013. Late Miocene-Middle Pleistocene sequences in the Po Plain-Northern Adriatic Sea (Italy): the stratigraphic record of modification phases affecting a complex foreland basin. Mar. Pet. Geol. 42, 50–81. https://doi.org/10.1016/j.marpetgeo.2012.11.007.

Goren, L., Fox, M., Willett, S.D., 2014. Tectonics from fluvial topography using formal linear inversion: Theory and applications to the Inyo Mountains, California. J. Geophys. Res. Earth 119 (8), 1651–1681. https://doi.org/10.1002/2014JF003079.

Howard, A., 1994. A detachment-limited model of drainage basin evolution. Water Resour. Res. 30 (7), 2261–2285. https://doi.org/10.1029/94WR00757.

Irace, A., Dela Pierre, F., Clari, P., 2005. "Normal" and "chaotic" deposits in the Messinian Gessoso-solfifera Fm. At the north-eastern border of the Langhe domain (Tertiary Piedmont basin). Ital. J. Geosci. 4, 77–85.

Irace, A., Clemente, P., Piana, F., De Luca, D.A., Polino, R., Violanti, D., Mosca, P., Trenkwalder, S., Natalicchio, M., Ossella, L., Governa, M., Petricig, M., 2010. Hydrostratigraphy of the late Messinian–Quaternary basins in the southern Piedmont (northwestern Italy). Memorie Descrittive della Carta Geologica d'Italia 90, 133–152.

Irace, A., Monegato, G., Tema, E., Martinetto, E., Gianolla, D., Vassio, E., Bellino, L., Violanti, D., 2015. Unconformity-bounded stratigraphy in the Plio-Pleistocene continental record: new insights from the Alessandria Basin (NW Italy). Geol. J. 52, 177–206. https://doi.org/10.1002/gj.2744.

Keller, E.A., Pinter, N., 2002. Active Tectonics, Earthquakes, Uplift and Landscape, 2nd edition. Prentice Hall, Upper Saddle River, p. 362.

Kirby, E., Whipple, K., 2012. Expression of active tectonics in erosional landscapes. J. Struct. Geol. 44, 54–75. https://doi.org/10.1016/j.jsg.2012.07.009.

Lanari, R., Reitano, R., Faccenna, C., Piana Agostinetti, N., Ballato, P., 2023. Surface and crustal response to deep subduction dynamics: Insights from the Apennines, Italy. Tectonics 42 (3). https://doi.org/10.1029/2022TC007461.

Laubscher, H., Biella, G.C., Cassinis, R., Gelati, R., Lozej, A., Scarascia, S., Tabacco, I., 1992. The collisional knot in Liguria. Geol. Rundsch. 81, 275–289.

Livani, M., Scrocca, D., Arecco, P., Doglioni, C., 2018. Structural and stratigraphic control on salient and recess development along a thrust belt front. The northern Apennines (Po Plain, Italy). J. Geophys. Res. Solid Earth 123 (5), 4360–4387. https://doi.org/10.1002/2017JB015235.

Marder, E., Gallen, S.F., 2023. Climate control on the relationship between erosion rate and fluvial topography. Geology. https://doi.org/10.1130/G50832.1.

McNab, F., Ball, P.W., Hoggard, M.J., White, N.J., 2018. Neogene Uplift and Magmatism of Anatolia; insights from drainage analysis and basaltic geochemistry. Geochem. Geophys. Geosyst. 19 (1), 175–213. https://doi.org/10.1002/2017GC007251.

Molli, G., Crispini, M., Mosca, P., Piana, F., and Federico, L. (2010). Geology of the Western Alps-Northern Apennine junction area: a regional review. Journal of the Virtual Explorer, Electronic Edition, ISSN 1441–8142, volume 36, paper 9 In: (Eds.) Marco Beltrando, Angelo Peccerillo, Massimo Mattei, Sandro Conticelli, and Carlo Doglioni, The Geology of Italy, 2010.

Mosca, P. (2006). Neogene Basin evolution in the western Po Plain (NW Italy): insights from seismic interpretation, subsidence analysis and low temperature (U-Th)/he thermochronology. [PhD thesis, Vrije Universiteit Amsterdam] Netherlands Research School Geology (NSG).

Mosca, P., Polino, R., Rogledi, S., Rossi, M., 2009. New data for the kinematic interpretation of the Alps–Apennines junction (Northwestern Italy). Int. J. Earth Sci. 99, 833–849. https://doi.org/10.1007/s00531-009-0428-2.

Mutti, E., Papani, L., Di Biase, D., Davoli, G., Mora, S., Segadelli, S., Tinterri, R., 1995. Il Bacino Terziario Epimesoalpino e le sue implicazioni sui rapporti tra Alpi ed Appennino. Mem. Soc. Geol. It. 47, 217–244.

Patacca, E., Sartori, R., Scandone, P., 1993. Tyrrhenian Basin and Apennines. Kinematic Evolution and Related Dynamic Constraints. In: Boschi, E., Mantovani, E., Morelli, A. (Eds.), Recent Evolution and Seismicity of the Mediterranean Region, NATO ASI Series. Springer, Netherlands, Dordrecht, pp. 161–171. https://doi.org/10.1007/978-94-011-2016-6_7.

Pavano, F., Gallen, S.F., 2021. A geomorphic examination of the Calabrian forearc translation. Tectonics 40, e2020TC006692. https://doi.org/10.1029/2020TC006692.

Pazzaglia, F.J., Fisher, J., 2022. A reconstruction of Apennine uplift history and the development of transverse drainages from longitudinal profile inversion. In: Koeberl, C., Claeys, P., Montanari, S. (Eds.), From the Guajira Desert to the Apennines, and from Mediterranean Microplates to the Mexican Killer Asteroid (Geol. Soc. Am. Spec. Pap. 557, 000-000). Geological Society of America.

Perron, J.T., Royden, L., 2013. An integral approach to bedrock river profile analysis. Earth Surf. Process. Landf. 38, 570–576. https://doi.org/10.1002/esp.3302.

Piana, F., Polino, R., 1995. Tertiary structural relationships between Alps and Apennines: the critical Torino Hill and Monferrato area. Northwestern Italy. Terra Nova 7 (2), 138–143. https://doi.org/10.1111/j.1365-3121.1995.tb00682.x.

Pieri, M., Groppi, G., 1981. Subsurface geological structure of the Po Plain. In C.N.R. (Ed.). Progetto Finalizzato Geodinamica 414, 1–13.

Pritchard, D., Roberts, G.G., White, N.J., Richardson, C.N., 2009. Uplift histories from river profiles. Geophys. Res. Lett. 36, L24301. https://doi.org/10.1029/2009GL040928.

Quye-Sawyer, J., Whittaker, A., Roberts, G., 2020. Calibrating fluvial erosion laws and quantifying river response to faulting in Sardinia Italy. Geomorphology 370, 107388. https://doi.org/10.1016/j.geomorph.2020.107388.

Racano, S., Schildgen, T.F., Consentino, D., Miller, S.R., 2021. Temporal and spatial variations in rock uplift from river-profile inversions at the Central Anatolian plateau southern margin. J. Geophys. Res. Earth 126, e2020JF006027. https://doi.org/10.1029/2020JF006027.

Racano, S., Schildgen, T., Ballato, P., Yildirim, C., Wittmann, H., 2023. Rock-uplift history oh the Central Pontides from river-profile inversions and implications for development of the North Anatolian Fault. Earth Planet. Sci. Lett. 616, 118231 https://doi.org/10.1016/j.epsl.2023.118231.

Roberts, G.G., White, N., 2010. Estimating uplift rate histories from river profiles using African examples. J. Geophys. Res. 115, B02406. https://doi.org/10.1029/2009JB006692.

Rossi, M., Minervini, M., Ghielmi, M., Rogledi, S., 2015. Messinian and Pliocene erosional surfaces in the Po Plain-Adriatic Basin: Insights from allostratigraphy and sequence stratigraphy in assessing play concepts related to accommodation and gateway turnarounds in tectonically active margins. Mar. Pet. Geol. 66 (1), 192–216. https://doi.org/10.1016/j.marpetgeo.2014.12.012.

Royden, L.H., 1993. Evolution of retreating subduction boundaries formed during continental collision. Tectonics 12, 629–638. https://doi.org/10.1029/92TC02641.

Rudge, J.F., Gareth, G.G., White, N.J., Richardson, C.N., 2015. Uplift histories of Africa and Australia from linear inverse modeling of drainage inventories. J. Geophys. Res. Earth 120 (5), 894–914. https://doi.org/10.1002/2014JF003297.

San Jose, M., Caves Rugenstein, J., Cosentino, D., Faccenna, C., Fellin, M.G., Ghinassi, M., Martini, I., 2020. Stable isotope evidence for rapid uplift of the central Apennines since the late Pliocene. Earth Planet. Sci. Lett. 544, 116376 https://doi.org/10.1016/j.epsl.2020.116376.

Schildgen, T.F., van der Beek, P.A., D'Arcy, M., Roda-Boluda, D., Orr, E.N., Wittmann, H., 2022. Quantifying drainage-divide migration from orographic rainfall over geologic timescales: Sierra de Aconquija, southern Central Andes. Earth Planet. Sci. Lett. 579, 117345 https://doi.org/10.1016/j.epsl.2021.117345.

Schwanghart, W., Scherler, D., 2014. Short communication: TopoToolbox 2—MATLAB-based software for topographic analysis and modeling in Earth surface sciences. Earth Surf. Dyn. 2 (1), 1–7. https://doi.org/10.5194/esurf-2-1-2014.

Sharma, H., Ehlers, T.A., Glotzbach, C., Schmid, M., Tielbörger, K., 2021. Effect of rock uplift and Milankovitch timescale variations in precipitation and vegetation cover on catchment erosion rates. Earth Surf. Dynam. 9, 1045–1072. https://doi.org/10.5194/esurf-9-1045-2021.

Smith, A.G.G., Fox, M., Schwanghart, W., 2022. Comparing methods for calculating channel steepness index. Eath-Sci. Rev. 227, 103970 https://doi.org/10.1016/j.earscirev.2022.103970.

Tucker, G.E., Whipple, K.X., 2002. Topographic outcomes predicted by stream erosion models: Sensitivity analysis and intermodal comparison. J. Geophys. Res. Solid Earth 107 (B9). https://doi.org/10.1029/2001JB000162. ETG 1-1-ETG 1-16.

Vigna, B., Fiorucci, A., Ghielmi, M., 2010. Relations between stratigraphy, groundwater flow and hydrogeochemistry in Poirino Plateau and Roero areas of the Tertiary Piedmont Basin, Italy. Memorie descrittive della Carta Geologica d'Italia 90, 267–292.

Whipple, K.X., 2004. Bedrock rivers and the geomorphology of active tectonics. Annu. Rev. Earth Planet. Sci. 32 (1), 151. https://doi.org/10.1146/annurev.earth.32.101802.120356.

Whipple, K.X., Tucker, G.E., 1999. Dynamics of the stream-power river incision model: Implications for height limits of mountain ranges, landscape response timescales, and research needs. J. Geophys. Res. 104 (B8), 17661–17674. https://doi.org/10.1016/j.earscirev.2016.06.001.

Whipple, K.X., Forte, A.M., DiBiase, R.A., Gasparini, N.M., Ouimet, W.B., 2017. Timescales of landscape response to divide migration and drainage capture: Implications for the role of divide mobility in landscape evolution. J. Geophys. Res. Earth 122, 248–273. https://doi.org/10.1002/2016JF003973.

Wobus, C.W., Tucker, G.E., Anderson, R.S., 2006. Self-formed bedrock channels. Geophys. Res. Lett. 33 (18) https://doi.org/10.1029/2006GL027182.

Wortel, M., Spakman, W., 2001. Subduction and slab detachment in the Mediterranean-Carpathian region. Science 291. https://doi.org/10.1126/science.290.5498.1910.

York, D., Evensen, N.M., Lopez Martínez, M., De Basabe Delgado, J., 2004. Unified equations for the slope, intercept, and standard errors of the best straight line. Am. J. Phys. 72, 367. https://doi.org/10.1119/1.1632486.